Indian Journal of Chemistry
Vol. 55A, May 2016, pp. 566-570

Synthesis of heteroatom-doped ZnO nanoparticles as an efficient visible light photocatalyst and its photoelectrochemical performance

Wenjie Wu, Xiaodan Zhu, Qiaoqiao Yin, Linxiang Tan, Xiaoxia Ke & Ru Qiao*

College of Chemistry and Life Sciences, Zhejiang Normal University, Jinhua 321004, China

Email: qiaoru@zjnu.cn

Received 21 December 2015; revised and accepted 28 April 2016

Heteroatom-doped ZnO nanoparticles ($Zn_{1-x}Ni_xO$ NPs) have been synthesized by a simple solvothermal approach. The photocatalytic activity of the products has been evaluated by a photoassisted degradation of Rhodamine B in aqueous solution under visible light irradiation. All the heteroatom-doped semiconductors exhibit better photocatalytic activities than pure ZnO, with the 1 mol% Ni^{2+}-doped ZnO showing the best photocatalytic activity. From the transient photocurrent response and electrochemical impedance spectroscopic experiments it is observed that the photogenerated charges of the Ni-doped ZnO show longer lifetime and higher separation than that of pure ZnO, leading to its superior visible light photoactivity. The active species tests indicate that the hydroxyl radical and active holes were primarily responsible for the enhanced photocatalytic performance of Rhodamine B, and the superoxide radical takes part partially in the oxidation process. A possible photocatalytic mechanism is proposed. Good photostability and reusability of the product show that the studied nanoparticles have potential application in dye wastewater treatment.

Keywords: Catalysts, Photocatalysts, Zinc oxide, Ni doping, Nanoparticles, Photoelectrochemical properties

Photocatalytic degradation of organic compounds on semiconductors offers a viable approach to solve a variety of environmental problems. Among the photocatalysts used, ZnO is a transparent semiconductor with a wide band gap and a large exciton binding energy, which makes it suitable for a wide range of applications, such as a photocatalyst, gas sensor, UV emitter, and so on.[1-3] However, ZnO is limited by its intrinsic drawbacks of quick recombination of photoinduced carriers and its poor absorption ability of visible light.[4] In order to utilize solar radiation more effectively, the development of narrowing the band gap of ZnO or splitting it into several sub-gaps is necessary. Among the various methods for improving ZnO catalytic activity[5-7], modification of ZnO by doping with heteroatoms is a suitable method to inhibit the recombination of photoinduced electron and holes and to promote photocatalytic activity. Mn^{2+}, Sn^{4+}, Cd^{2+}, Cu^{2+}, Co^{2+} and some other metal ions[8-12] are often used as attractive dopants for ZnO because they are isomorphic to Zn^{2+} ions.

Herein, we report our recent efforts on synthesis of the Ni-doped ZnO nanoparticles ($Zn_{1-x}Ni_xO$ NPs) through a solvothermal process. The visible light photocatalytic activity of the $Zn_{1-x}Ni_xO$ NPs was evaluated by the degradation of Rhodamine B (RhB) as a model reaction. It was found that the doped oxide possesses better visible light photocatalytic activity than pure ZnO synthesized through the same approach. The effect of doping content on enhanced photodegradation performance of the doped oxides was further studied. In addition, transient photocurrent response and electrochemical impedance spectroscopic (EIS) techniques were performed to study the effect of Ni^{2+}-doping on the efficient separation of photogenerated charge carriers and also the kinetic process of the electron and hole transmission. Reactive active species involved in the photodegradation process was determined through a set of scavenger experiments. The photocatalytic mechanism of $Zn_{1-x}Ni_xO$ for organic dye degradation is proposed.

Experimental

Ni-doped ZnO NPs were synthesized via a solvothermal method reported in our previous work.[13] Briefly, 4.95 mmol of $Zn(Ac)_2{\cdot}2H_2O$ and 0.05 mmol of $Ni(Ac)_2{\cdot}4H_2O$ were dissolved in ethylene glycol-H_2O (EG-H_2O, *v/v*, 1:1) mixed solvent with stirring for 0.5 h at 0 °C. NaOH (50 mmol) was added to the above solution with stirring for another 1 h. Subsequently, the suspension was taken in a 50 mL Teflon-lined autoclave and heated at 200 °C for 2 h followed by naturally cooling to room temperature. The precipitates were collected and washed with ethanol, then dried at 60 °C. For comparison, $Zn_{1-x}Ni_xO$ samples with different Ni-doping contents from 0 to 6 mol% were also synthesized by the same method.

The microstructures of the products were analyzed by scanning electron microscopy (SEM, JEOL

JSM-6700F) and transmission electron microscopy (TEM, JEOL 2010F). Photoluminescence (PL) spectra of the oxide NPs were recorded at room temperature using Edinburgh FLS 920 fluorescence spectrophotometer.

A Xenon lamp (HSX-UV300W, NBet) with a UV cut-off filter (400 nm) acted as a visible light source. The catalyst (20 mg) was dispersed in 100 mL of aqueous RhB (10 mg L^{-1}). Before irradiation, the suspension was magnetically stirred in dark for 30 min to ensure adsorption-desorption equilibrium on the surface of the $Zn_{1-x}Ni_xO$. During irradiation, 5 mL of sample aliquots were extracted at 30 min intervals. After removing any solid suspension by centrifugation, the decomposition of RhB was followed spectrophotometrically (UV-vis spectrophotometer; TU-1810, Puxi).

In addition, to understand the kinds of reactive species directly taking part in the RhB photocatalytic degradation over $Zn_{1-x}Ni_xO$ sample under visible light irradiation, an identical set of radical scavenger experiments[14-16] were performed with $Zn_{0.99}Ni_{0.01}O$, in which the photodegradation of RhB was repeated with modification by adding 15 mg of *p*-benzoquinone (PBQ) as a superoxide radical ($\cdot O_2^-$) scavenger or 15 mg of *t*-butylalcohol (TBA) as a hydroxyl radical ($^{\cdot}OH$) scavenger or 15 mg of ethylenediamine tetraacetic acid (EDTA) as an h^+ scavenger.

For the reuse test, the photocatalyst was recollected by centrifugation and redispersed in the fresh dye solution, followed by testing of the photocatalytic activity via the above method.

The photocurrent measurements were made on a conventional three-electrode system (CHI 660B) with a Pt wire as the counter electrode and Ag/AgCl (saturated KCl) as the reference electrode. The light source was a 300 W Xenon lamp equipped with a UV cut-off filter ($\lambda > 420$ nm), and the electrolyte was 0.2 *M* Na_2SO_4. The working electrode was the resulting sample film (effective surface area about 2×0.5 cm^2), which was illuminated from the FTO glass side. Electrochemical impedance spectroscopy (EIS) data were obtained with the above three-electrode system, in the frequency range of 0.01–10^5 Hz with an AC amplitude of 10 mV at 0.2 V.

Results and discussion

Figure 1a shows the SEM image of Ni-doped ZnO NPs revealing a relatively uniform size population with main diameter of ~100 nm. The particles have a rather smooth surface and reveal a hexagonal-based polyhedron structure resulting from low anisotropic growth rate in the mixed solvent with low polarity (Inset of Fig. 1a). The interplanar spacing for all lattice fringes is 0.261 nm, which corresponds to [001] direction of ZnO (Fig. 1b). The selected area electron diffraction (SAED) pattern shows strong diffused spots rather than weak diffused rings, indicating that the doped ZnO has single crystalline

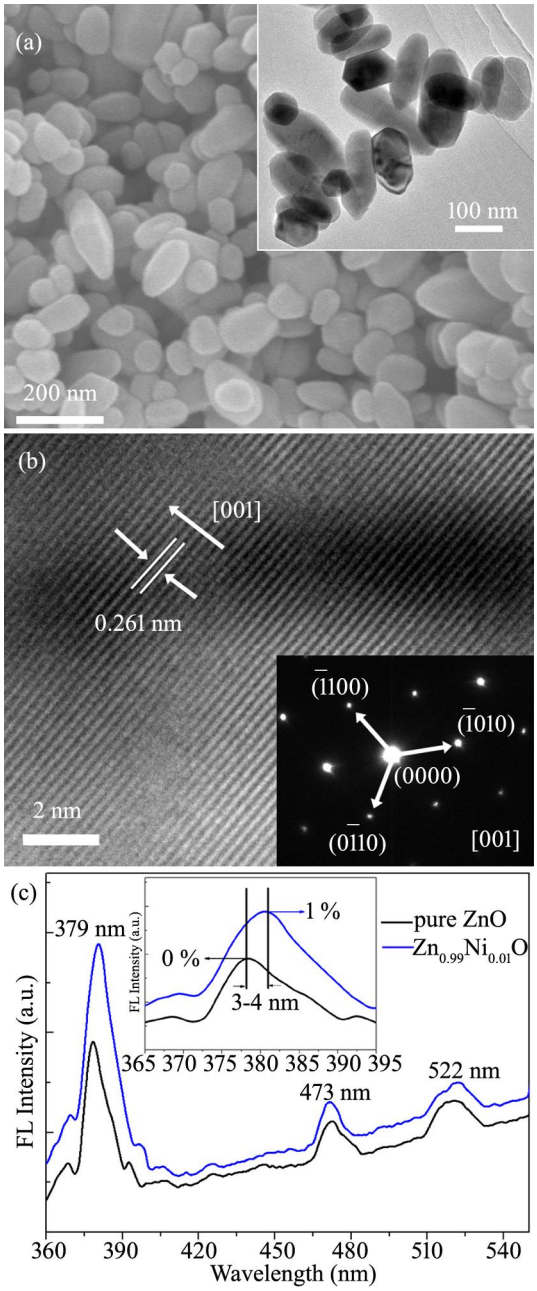

Fig. 1—(a) SEM and (b) HRTEM images of the $Zn_{0.99}Ni_{0.01}O$. [Inset of (a) and (b) are its TEM image and SAED pattern, respectively]. (c) Room temperature PL spectra of ZnO and $Zn_{0.99}Ni_{0.01}O$ under 325 nm excitation.

nature and is orderly arranged along the [001] direction (inset of Fig. 1b). As shown in Fig. 1c, the PL spectra consist of a UV emission peak centered at 379 nm, a weaker blue-green emission band centered at 473 nm, and a distinct green emission band centered at 522 nm, respectively. The UV luminescence band (379 nm) is assigned to the near-band-edge emission of ZnO. A red shift of ~3-4 nm can be observed (inset of Fig. 1c), which suggests the decreased band gap on Ni doping. The visible emissions (473 nm and 522 nm) are generally defined as the radial recombination of photogenerated electron-hole (e^--h^+) pair from deep levels in the band gap, resulting in lower energy emission. These deep level emissions are attributed to the defects, such as O-vacancy and Zn-vacancy, in the crystal created by the dopant. In addition, surface states have also been identified as a possible cause of the visible emission in ZnO nanomaterials.[17]

The photocatalytic activities at different doping concentrations, ranging from 0.5 mol% to 6 mol%, of $Zn_{1-x}Ni_xO$ photocatalysts are shown in Fig. 2. The photodegradation results reveal that all $Zn_{1-x}Ni_xO$ samples exhibit higher photocatalytic efficiencies than pure ZnO. It is generally accepted that the photocatalytic activity depends mainly on the effective separation of photoinduced electrons and holes. To illustrate the generation and transfer of photoexcited charge carriers in the photodegradation process, the transient photocurrents of the semiconductors were investigated during repeated ON/OFF illumination cycles. From photocurrent versus time curves (Fig. 3a), one can observe that both the doped ZnO and pure ZnO exhibit reproducible photocurrent response at each illumination pulse. For the 1 mol% Ni-doped ZnO sample ($Zn_{0.99}Ni_{0.01}O$), a sharp increase in photocurrent appeared once the Xe lamp irradiation was switched on, and when the irradiation was interrupted the photocurrent rapidly dropped to a steady state value. The generated photocurrent of $Zn_{0.99}Ni_{0.01}O$ induced by visible light illumination reached 0.07 mA cm^{-2}; almost 2.5 times higher than that of pure ZnO (0.028 mA·cm^{-2}). It is known that the higher the photocurrent, the higher the electron-hole separation efficiency, and hence, the higher the photocatalytic activity. The enhanced photocurrent of the heteroatom-doped ZnO implies that its photoinduced electron transfer was more efficient than that of pure ZnO, which is beneficial for enhancing the photocatalytic activity.

The electrochemical impedance spectroscopic (EIS) technique was used to analyze the charge carrier transport in the samples. In Nyquist diagrams, the radii of the arcs are associated with the charge transfer at the interface between the electrode and electrolyte

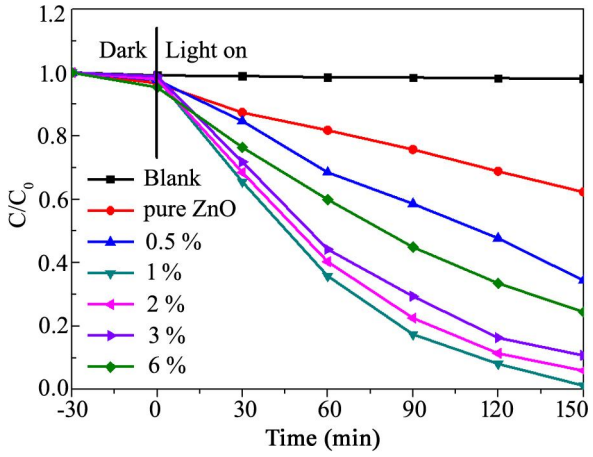

Fig. 2—Photodegradation of Rh B under visible light irradiation in the presence of $Zn_{1-x}Ni_xO$ with different dopant contents from 0–6 mol%.

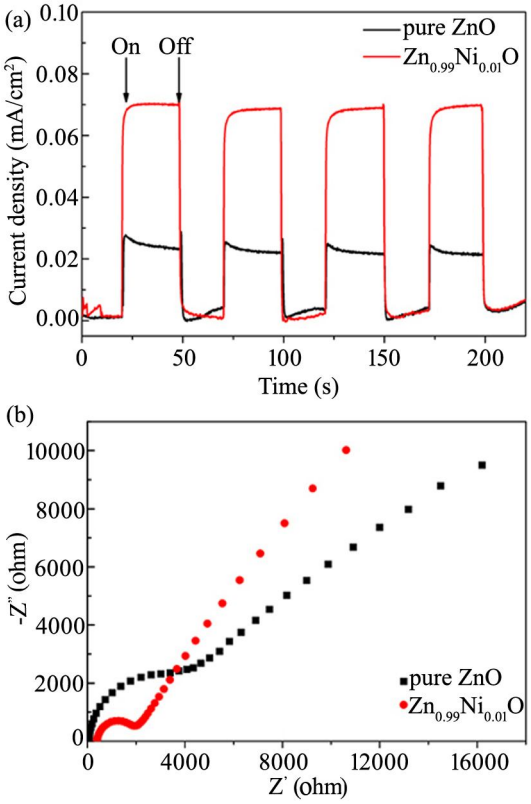

Fig. 3—(a) Transient photocurrent density versus time plots for ZnO and $Zn_{0.99}Ni_{0.01}O$ samples. (b) EIS Nyquist plots of ZnO and $Zn_{0.99}Ni_{0.01}O$ samples under visible light illumination.

solution. A smaller radius corresponds to lower charge transfer resistance.[18,19] As shown in Fig. 3b, the arc radius of the EIS Nyquist plot of the $Zn_{0.99}Ni_{0.01}O$ was smaller than that of ZnO, demonstrating that the Ni-doped ZnO NPs exhibit lower charge transfer resistance, which explains its better photoresponse shown in Fig. 3a. Overall, this implies that substantial shuttling of charges between the electrode and electrolyte and faster interfacial charge transfer occurred at the composite interface, which lowers the recombination probability of photogenerated electrons and holes and hence increases the photocatalytic activity.

The concentration effect shows that the optimum doping concentration of Ni^{2+} in ZnO is 1 mol% (Fig. 2). At low doping concentration (less than or equal to 1 mol%), the doped Ni^{2+} ions act as mediator of interfacial charge transfer, which can efficiently prevent the possibility of recombination of photogenerated electrons and holes. At doping higher than 1 mol%, the recombination rate will increase because the distance between trapping sites in a particle decreases, making the transition metal ions substituted in ZnO lattice act as recombination centers for electrons and holes.

To investigate the proposed photocatalytic mechanism of the $Zn_{0.99}Ni_{0.01}O$ hybrid, the influence of various radical scavengers on the rate of the photodegradation of RhB under visible light irradiation over $Zn_{0.99}Ni_{0.01}O$ was examined. The results of radical scavenger experiments are displayed in Fig. 4. As seen in Fig. 4, RhB decolorization was strongly inhibited in the presence of TBA as a diagnostic tool, and the photodegradation of RhB was only 31.4%, which is much lower than in the absence of TBA. This confirms that the hydroxyl radical is indeed an active species in the RhB degradation process over the $Zn_{0.99}Ni_{0.01}O$ catalyst. An additional test was performed with PBQ to further explore the role of the superoxide radical . When PBQ was added, the photodegradation of RhB was inhibited slightly, but was higher than that in the presence of TBA, indicating the $\cdot O_2^-$ was not the main active species involved in RhB degradation. On the other hand, the degradation rate of RhB with $Zn_{0.99}Ni_{0.01}O$ was inhibited significantly with the addition of EDTA, a well-known scavenger of h^+, indicating that the h^+ also played a key role in the RhB degradation.

Thus, it is believed that ·OH and h^+ are the main active species in the degradation of RhB, and the

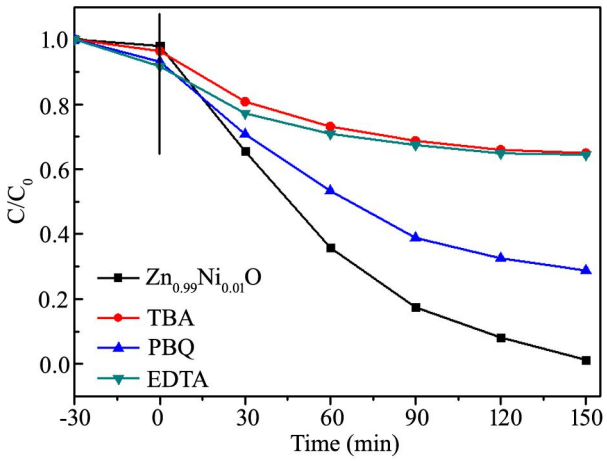

Fig. 4—Effects of various scavengers on the degradation of RhB in the presence of $Zn_{0.99}Ni_{0.1}O$.

generated $\cdot O_2^-$ radicals partially take part in the oxidation. Based on the results of scavenger experiments, a possible reaction mechanism for the superior photocatalytic activity of $Zn_{0.99}Ni_{0.01}O$ is summarized in Scheme 1.

$$Zn_{0.99}Ni_{0.01}O + h\nu \rightarrow Zn_{0.99}Ni_{0.01}O\ (e_{CB}^- + h_{VB}^+) \quad ...(1)$$

$$h_{VB}^+ + H_2O \rightarrow \cdot OH + H^+ \quad ...(2)$$

$$e_{CB}^- + O_2 \rightarrow \cdot O_2^- \quad ...(3)$$

$$e_{CB}^- + \cdot O_2^- + 2H^+ \rightarrow H_2O_2 \quad ...(4)$$

$$H_2O_2 + e_{CB}^- \rightarrow \cdot OH + OH^- \quad ...(5)$$

$$h_{VB}^+ + OH^- \rightarrow \cdot OH \quad ...(6)$$

$$RhB + \cdot OH \text{ and } \cdot O_2^- \rightarrow \text{degradation products} \quad ...(7)$$

$$RhB + h_{VB}^+ \rightarrow \text{degradation products} \quad ...(8)$$

Scheme 1

The stability and reusability of the $Zn_{0.99}Ni_{0.01}O$ sample were evaluated by photodegradation of RhB under visible light irradiation repeated for five recycles. $Zn_{0.99}Ni_{0.01}O$ exhibits excellent photostability as the RhB degradation was 98.8, 95.1, 91.3, 87.9 and 84.4% for 1-5 recycles, respectively. This result indicates that the $Zn_{0.99}Ni_{0.01}O$ photocatalyst can be utilized repeatedly with potential application in the industrial field. A slight reduction of the photocatalytic activity may be due to incomplete collection of the sample by centrifugation.

In summary, $Zn_{1-x}Ni_xO$ NPs were obtained via a one-step solvothermal method. The samples showed greatly enhanced photocatalytic activity under visible light irradiation. The 1 mol% Ni-doped ZnO exhibited the best photocatalytic performance. The high activity may be ascribed to enhanced photogenerated charge separation and charge transfer as shown by transient

photocurrent response and EIS measurements. OH and h^+ are confirmed to be the main active species in the degradation of RhB based on the radical scavenger experiments. The recycling test confirmed the good photostability and reusability of the photocatalyst.

Acknowledgement

This work is financially supported by the National Natural Science Foundation of China (grant No. 21201151) and the Natural Science Foundation of Zhejiang Province (grant No. LY15B010003).

References

1 Xu L, Hu Y L, Pelligra C, Chen C H, Jin L, Huang H, Sithambaram S, Aindow M, Jeosten R & Suib S L, *Chem Mater*, 21 (2009) 2875.
2 Pan X, Liu X, Bermak A & Fan Z, *ACS Nano*, 7 (2013) 9318.
3 Ouyang G & Yang G W, *ACS Appl Mater Interfaces*, 4 (2012) 210.
4 Yin Q, Qiao R, Zhu L, Li Z, Li M & Wu W, *Mater Lett*, 135 (2014) 135.
5 Darvishi C S R, Rezaee A, Khataee A R & Safari M, *J Ind Eng Chem*, 20 (2014) 1861.
6 Habibi M H & Habibi A H, *J Ind Eng Chem*, 20 (2014) 68.
7 Li B, Hu G S, Jin L Y, Hong X, Lu J Q & Luo M F, *J Ind Eng Chem*, 19 (2013) 250.
8 Yang Y, Li Y, Zhu L, He H, Hu L, Huang J, Hu F, He B & Ye Z, *Nanoscale*, 5 (2013) 10461.
9 Karunakaran C, Sakthi Raadha S, Gomathisankar P & Vinayagamoorthy P, *Dalton Trans*, 42 (2013) 13855.
10 Peng Y, Qin S, Wang W S & Xu A W, *CrystEngComm*, 15 (2013) 6518.
11 Lu Y H, Lin W H, Yang C Y, Chiu Y H, Pu Y C, Lee M H, Tseng Y C & Hsu Y J, *Nanoscale*, 6 (2014) 8796.
12 Kuriakose S, Satpati B & Mohapatra S, *Phys Chem Chem Phys*, 16 (2014) 12741.
13 Zhang X L, Qiao R, Kim J C & Kang Y S, *Cryst Growth Des*, 8 (2008) 2609.
14 Li X, Mao X, Zhang X, Wang Y, Wang Y, Zhang H, Hao X & Fan C, *Sci China Chem*, 58 (2015) 457.
15 Huang Y, Li H, Balogun M S, Liu W, Tong Y, Lu X & Ji H, *ACS Appl Mater Interfaces*, 6 (2014) 22920.
16 Jiang W, Wu Z, Yue X, Yuan S, Lu H & Liang B, *RSC Adv*, 5 (2015) 24064.
17 Peng Z, Dai G, Zhou W, Chen P, Wan Q, Zhang Q & Zou B, *Appl Surf Sci*, 256 (2010) 6814.
18 Bell N J, Ng Y H, Du A, Coster H, Smith S C & Amal R, *J Phys Chem C*, 4 (2011) 171.
19 Hou Y, Zuo F, Dagg A & Feng P, *Angew Chem Int Ed*, 52 (2013) 1248.